ADVANCED OPTICAL MATERIALS
www.advopticalmat.de

Chemical Group Substitution Enables Highly Efficient Mn^{4+} Luminescence in Heterovalent Systems

Hong Ming, Yifei Zhao, Yayun Zhou, Maxim S. Molokeev, Yuanjing Wang, Enhai Song,* and Qinyuan Zhang**

Defects are a double-edged sword for heterovalent metal-ion doping phosphors. Along with the luminescence tunability of phosphors bestowed by defects, their expected luminescence efficiency would also be inevitably lowered due to the presence of these quenching sites. Herein, a chemical group substitution strategy is proposed, where inorganic polyhedrons act as the smallest chemical units during the structural evolution of the doping process. Such a method can not only effectively prevent the defect generation for charge compensation in heterovalent doping systems, but also facilitate the incorporation of activators into the matrix, leading to extremely high luminescence efficiency. The concept is first confirmed energetically favorable by first-principles simulations. As a robust experimental proof, two newly reported Mn^{4+}-incorporated hexavalent organic-inorganic hybrid oxyfluorides $(TMA)_2BO_2F_4$:Mn^{4+} (where TMA stands for tetramethylammonium, and B = W^{6+} or Mo^{6+}) present high quantum efficiency (up to 94.4%) and short lifetime (down to 2.26 ms) that are superior to the commercial red phosphor K_2SiF_6:Mn^{4+} (≈84.8%, ≈8.06 ms). Utilizing the differences in decay lifetimes and thermal quenching behaviors of $(TMA)_2BO_2F_4$:Mn^{4+} and K_2SiF_6:Mn^{4+}, a time- and temperature-resolved single-color multiplexing mode with high-safety and easy-access is developed for information security. This work offers an effective strategy to manipulate defect generation in luminescent materials.

1. Introduction

Luminescent materials (or phosphors) based on activators have been widely used in the fields of solid-state lighting, display, anti-counterfeiting, information storage, and photoelectric detection due to their rich and tunable luminescence properties.[1–4] To obtain high luminescence efficiency, the activator ions are commonly introduced into the equivalent cationic site to avoid the generation of charge compensation defects (i.e., quenching sites), where the excitation energy is lost non-radiatively (as heat).[5–7] On the other hand, as evidenced by many types of research, the incorporation of activators into a heterovalent site can also be regarded as a powerful approach to developing a high-performance phosphor, namely the heterovalent doping scheme.[8–11] Compared with the equivalent doping, heterovalent doping can induce some abnormal local environments around the activators, leading to the emergence of new fascinating luminescent properties (e.g., new emission band, zero thermal quenching, and shortened fluorescence lifetimes).[12–14] However, the inevitable co-existence of defects to maintain the charge balance is detrimental to the overall performance of phosphors, particularly in terms of quantum efficiencies (QEs). Therefore, the design principle to avoid the generation of charge compensation defects is urgently required for the heterovalent doping phosphors.

Mn^{4+}-doped fluoride phosphors have received enormous attention in display and lighting due to the broadband

H. Ming, Y. Zhao, Y. Zhou, Y. Wang, E. Song, Q. Zhang
State Key Laboratory of Luminescent Materials and Devices
Guangdong Provincial Key Laboratory of Fiber Laser Materials and Applied Techniques, and Guangdong Engineering Technology Research and Development Center of Special Optical Fiber Materials and Devices
South China University of Technology
Guangzhou 510641, P. R. China
E-mail: zhou-yayun@foxmail.com; msehsong@scut.edu.cn; qyzhang@scut.edu.cn

M. S. Molokeev
Laboratory of Crystal Physics
Kirensky Institute of Physics
Federal Research Center KSC SB RAS
Krasnoyarsk 660036, Russia

M. S. Molokeev
Institute of Engineering Physics and Radioelectronics
Siberian Federal University
Krasnoyarsk 660041, Russia

M. S. Molokeev
Department of Physics
Far Eastern State Transport University
Khabarovsk 680021, Russia

Q. Zhang
School of Physics and Optoelectronics
South China University of Technology
Guangzhou 510641, P. R. China

The ORCID identification number(s) for the author(s) of this article can be found under https://doi.org/10.1002/adom.202300076.

DOI: 10.1002/adom.202300076

blue-light absorption (≈450 nm) and narrowband red emission (≈630 nm).[15,16] Over decades of rapid development, the Mn^{4+}-doped fluoride family has extended from equivalent doping systems represented by K_2SiF_6:Mn^{4+} (KSF) to heterovalent doping systems like K_2NaAlF_6:Mn^{4+}.[6,17–19] Their story can provide a vivid picture of the gains and losses in QEs brought by charge compensation defects (Table S1 and Figure S1, Supporting Information). Compared to equivalent doping systems, the heterovalent counterparts usually possess short decay lifetimes which facilitates their application in displays.[14] However, the presence of defects for charge compensation, which play as luminescence quenching sites, leads to easy concentration quenching at low Mn^{4+} doping content.[14] It is thus hard to achieve high doping concentration in a heterovalent doping scheme and the overall luminescence efficiency is inferior. Several compensation methodologies, such as the heterovalent co-doping strategy (i.e., co-doping with charge compensators, or namely, co-substitution strategy), and surface passivation treatment, have been proposed to improve the QEs, whereas the outcomes are below expectations.[6,20] Therefore, it is still a great challenge to realize the simultaneous elimination of defects for charge compensation and achieving high Mn^{4+} doping concentration in heterovalent doping systems.

Mn^{4+} is an environmentally sensitive activator ion in the liquid phase and is susceptible to oxidation or reduction to other valence states, or hydrolysis to the manganese oxide MnO_2.[21,22] It cannot exist in solution alone stably and freely, but is dissolved in the form of complex ions, such as $Mn[HPO_4]_2$ in H_3PO_4 and $[MnF_6]^{2-}$ in HF solution.[23] Therefore, during the synthesis of Mn^{4+}-doped fluoride phosphors in HF solution, the activator Mn^{4+} is introduced to the matrixes in the form of $[MnF_6]^{2-}$ by replacing other chemical groups (such as $[SiF_6]^{2-}$ and $[AlF_6]^{3-}$), which we defined as the "chemical group substitution" (CGS) strategy. In that case, the presence of defect for charge compensation can be eliminated by employing matrixes that possess equivalent chemical groups $[BX_6]^{2-}$ to $[MnF_6]^{2-}$ in HF solution. No matter how B and X are composed, the $[MnF_6]^{2-}$ dopants are expected to be treated equally with $[BX_6]^{2-}$ octahedrons during the as-defined CGS process, thus no charge compensation is required. On the other hand, our previous research has shown that a discrete $[BX_6]^{2-}$ octahedral lattice framework is hard to achieve in conventional all-inorganic fluoride (or oxyfluoride) matrixes due to the small ionic radii of the alkali (or alkaline earth) metal ions.[24,25] The utilization of organic cationic groups with much larger ionic radii (steric hindrance) can effectively isolate the $[BX_6]^{2-}$ blocks, resulting in avoided Mn^{4+} agglomerations as well as suppressed Mn^{4+}-Mn^{4+} and Mn^{4+}-to-defect energy transfer. Accordingly, we adopted the as-proposed CGS strategy onto organic-inorganic hybrid oxyfluoride matrixes to achieve high-performance Mn^{4+}-activated heterovalent phosphors with higher Mn^{4+} doping concentration and without charge compensation defects.

In this work, we designed two novel Mn^{4+}-doped organic-inorganic hybrid heterovalent oxyfluoride phosphors $(TMA)_2BO_2F_4$:Mn^{4+} (where TMA stands for tetramethylammonium, and B is hexavalent metal ions W^{6+} and Mo^{6+}) by as-proposed CGS strategy. Both two heterovalent phosphors present high QE (up to 94.4%) and short lifetime (down to 2.26 ms) at high Mn^{4+} doping concentrations of ~10 mol% that are superior to the commercial K_2SiF_6:Mn^{4+} (≈84.8%, ≈8.06 ms). Their structures and luminescence properties were investigated in detail, where the mechanism for such big improvements of QEs compared to present all-inorganic heterovalent systems was unraveled. Besides the promising application prospects in wide-color gamut backlight display, taking advantage of the difference in luminescence properties between $(TMA)_2BO_2F_4$:Mn^{4+} and KSF, a novel time-resolved and temperature-resolved single-color multiplexing mode with high safety and easy access was developed for information security. This work not only brings a brand-new kind of Mn^{4+}-doped organic-inorganic hybrid oxyfluoride phosphors to the sight of the phosphor community but also provides a useful reference for the design of doping schemes toward highly efficient heterovalent doping luminescent materials.

2. Results and Discussion

To verify our hypothesis, herein, the as-proposed CGS strategy was examined in two newly discovered organic-inorganic hybrid oxyfluorides $(TMA)_2BO_2F_4$ (where TMA stands for tetramethylammonium, B = W^{6+} or Mo^{6+}) upon heterovalent Mn^{4+} doping. Density functional theory (DFT) simulation was first performed to evaluate the most stable doping models using the resolved crystal structures based on the single crystal X-ray diffraction (SCXRD) data of these two oxyfluorides (Figure S2 and Tables S2–S10, Supporting Information). Their crystallographic data are deposited in Cambridge Crystallographic Data Centre (CCDC 2205717–2205718). Taking $(TMA)_2WO_2F_4$ as the example, a series of models were established based on different charge compensation forms as illustrated in **Figure 1**a. Regarding the intrinsically disordered F/O layouts obtained from the SCXRD, some possible undoped structures with fixed atomic positions were first compared (Figure S3 and Table S11, Supporting Information). The one with adjacent O atoms in each polyhedron was found to have the lowest total energy, which is similar to all-inorganic oxyfluoride counterparts.[26–28] Therefore, it was employed as the pristine structure for further calculations. More detailed computation settings are provided in the Supporting Information. The defect formation energy (E^f) of each doping model was calculated and compared. Chemical group substitution of $[MnF_6]^{2-}$/$[WO_2F_4]^{2-}$ represented by case 1 appears as the most stable model, for its E^f is much lower than the ones representing conventional single ion substitution (case 6, one Mn''_W accompanied by two interstitial TMA), co-substitution (case 3 and case 4, one Mn''_W with two nearby F_O^-). Therefore, the as-proposed "chemical group substitution" is energetically favorable during Mn^{4+}-doping. Cases are similar in $(TMA)_2MoO_2F_4$ (Figure S4, Supporting Information). The reason can be attributed to the sterically large TMA cations in $(TMA)_2BO_2F_4$ that separate the inorganic blocks into a 0D framework, furnishing isolated-unit-like behaviors of the blocks.[29] Such strategy has also been examined valid in all-inorganic 0D $(NH_4)_2NbOF_5$ and $Rb_2MoO_2F_4$ with preferable $[MnF_6]^{2-}$/$[NbOF_5]^{2-}$ or $[MnF_6]^{2-}$/$[MoO_2F_4]^{2-}$ chemical group substitution, respectively (Figures S5 and S6, Supporting Information). In addition, the capability of $(TMA)_2BO_2F_4$ (B = W^{6+} or Mo^{6+}) to accommodate the Mn^{4+} impurity level

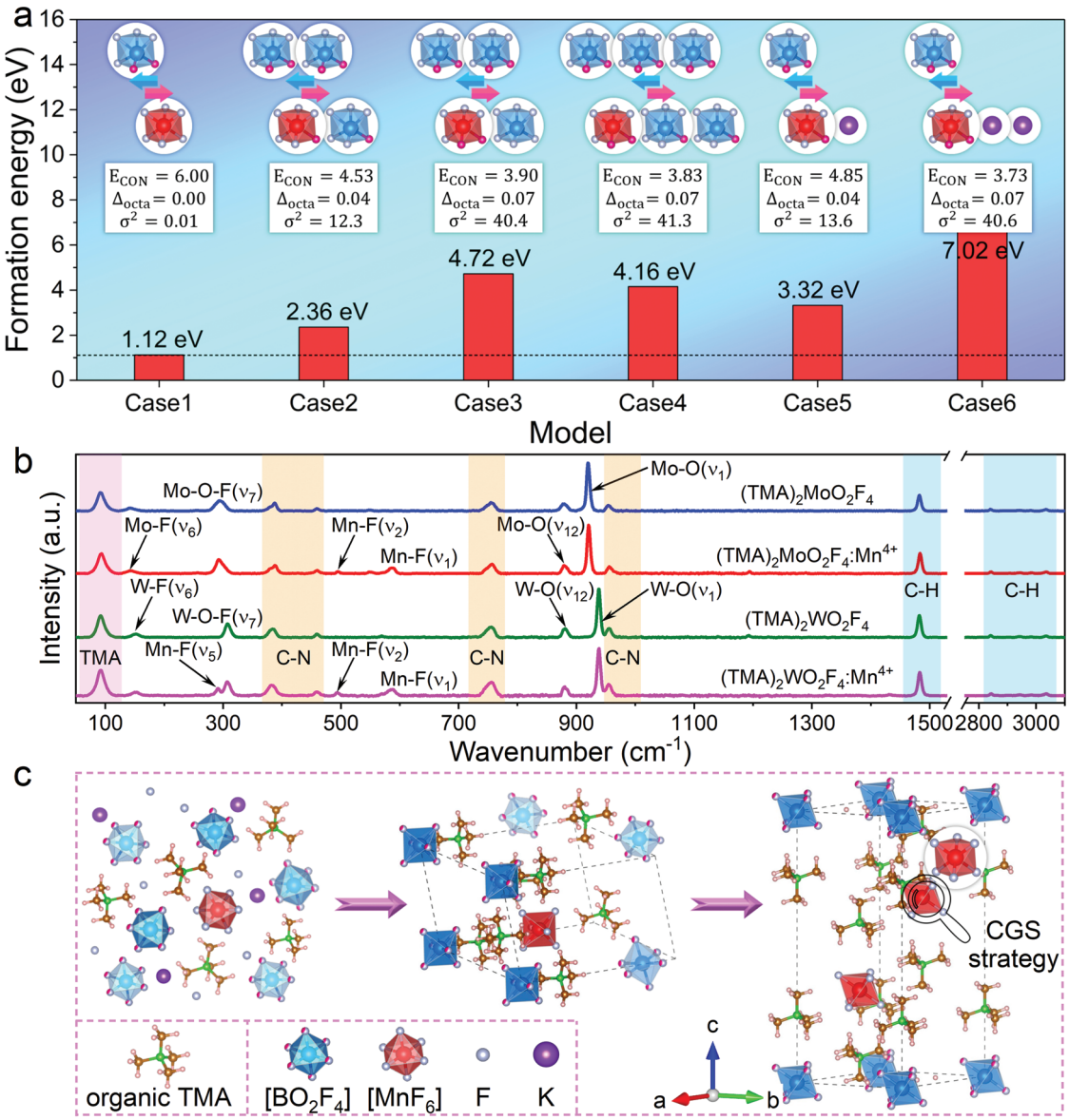

Figure 1. a) The formation energy diagram comparing each available doping model in $(TMA)_2WO_2F_4$:Mn^{4+}, the substitution ions, and resultant local symmetry factors of the corresponding model are listed in the upper diagram. b) The Raman spectra of $(TMA)_2BO_2F_4$:Mn^{4+} (B = W^{6+} or Mo^{6+}) and $(TMA)_2BO_2F_4$. c) Schematic illustration of the chemical group substitution (CGS) strategy during the synthesis of Mn^{4+}-doped $(TMA)_2BO_2F_4$ hybrid oxyfluoride phosphors.

was also examined (Figure S7, Supporting Information). As the calculated density of states shown in Figure S8, Supporting Information, the Mn^{4+} energy levels can be effectively sandwiched in the forbidden band of the host. After introducing Mn^{4+} impurity levels, the spin-polarized feature also matches well with the Mn^{4+} $3d^3$ electron configuration interpreted by the crystal field theory as represented by $(TMA)_2WO_2F_4$:Mn^{4+} (marked in Figure S8, Supporting Information). Theoretical simulation results also indicate a high symmetry of the $[MnF_6]$ groups in $(TMA)_2BO_2F_4$:Mn^{4+} according to the calculated distortion indices (E_{CON}, Δ_{octa}, and σ^2, as listed in the tables of each model in Figure 1a and Figure S4, Supporting Information), which can be evidenced by spectral analyses as will be discussed later.

The DFT simulation results were then confirmed by experimental characterizations. A series of Mn^{4+}-doped and undoped $(TMA)_2BO_2F_4$ powder samples were synthesized through a facile co-precipitation method (Figure S9, Supporting Information). All the XRD results match well with the simulated card from the corresponding SCXRD data with no sign of impurities (Figure S10, Supporting Information). The Raman and Fourier transform infrared spectra confirm the TMA, $[MnF_6]$, and $[BO_2F_4]$ groups on the hybrid structure as tagged in Figure 1b and Figure S11, Supporting Information. In addition, only typical signals of Mn-F can be observed from the Mn^{4+}-doped samples, whereas the absence of Mn-O vibronic modes at ≈510 or ≈630 cm^{-1} supported the successful chemical group substitution from an experimental perspective. The element composition

and the valance states of both two $(TMA)_2BO_2F_4$:Mn^{4+} were confirmed by X-ray photoelectron spectroscopy studies (Figure S12, Supporting Information). The possible procedure of Mn^{4+} incorporated into the $(TMA)_2BO_2F_4$ in the form of group substitution was schematically demonstrated in Figure 1c. Inorganic groups $[BO_2F_4]$ and $[MnF_6]$ co-exist with large organic TMA cationic groups in the solution system, which will further assemble into 0D-like structures before eventually precipitating as hybrid compound $(TMA)_2[BO_2F_4]_{1-x}[MnF_6]_x$ (x denotes the doping concentration). Taking $(TMA)_2WO_2F_4$:Mn^{4+} as the example, the reaction processes for the synthesis of $(TMA)_2BO_2F_4$:Mn^{4+} are as follows

$$H_2WO_4 + 4HF \rightarrow [WO_2F_4]^{2-} + 2H_2O + 2H^+ \quad (1)$$

$$K_2MnF_6 \rightarrow [MnF_6]^{2-} + 2K^+ \quad (2)$$

$$TMAF \cdot 4H_2O \rightarrow TMA^+ + F^- + 4H_2O \quad (3)$$

$$2TMA^+ + (1-x)[WO_2F_4]^{2-} + x[MnF_6]^{2-} \rightarrow (TMA)_2[WO_2F_4]_{1-x}[MnF_6]_x \quad (4)$$

When the raw material H_2WO_4 is added to the HF solution, it will be converted into $[WO_2F_4]^{2-}$ groups due to the higher electronegativity of F^- ions (Equation (1)). The dissolution and ionization of K_2MnF_6 and $TMAF \cdot 4H_2O$ will add $[MnF_6]^{2-}$ groups, K^+, TMA^+, and F^- into the above solution (Equations (2) and (3)). Further addition of excess $TMAF \cdot 4H_2O$ precipitant initiates the assemblage and precipitation of TMA^+, $[WO_2F_4]^{2-}$, and $[MnF_6]^{2-}$, resulting in the formation of intended hybrid compounds $(TMA)_2[BO_2F_4]_{1-x}[MnF_6]_x$ (Equation (4)). The charge conservation between $[WO_2F_4]^{2-}$ and $[MnF_6]^{2-}$ groups facilitates the incorporation of Mn^{4+} into the $(TMA)_2WO_2F_4$ lattice, resulting in a high Mn^{4+} doping concentration (Table S1, Supporting Information). The formation mechanism is likewise for $(TMA)_2MoO_2F_4$:Mn^{4+} (Supporting Information).

Both $(TMA)_2BO_2F_4$:Mn^{4+} show typical luminescence features of Mn^{4+} according to the photoluminescence excitation (PLE) and PL spectra in **Figure 2**a,b. The broad excitation bands (≈375 and ≈470 nm) originated from the $^4A_2 \rightarrow {}^4T_1$ and $^4A_2 \rightarrow {}^4T_2$ transitions, respectively, which matches well with main-stream light-emitting diode chips. The emission signals are assigned to the forbidden intra-configurational $^2E \rightarrow {}^4A_2$ transitions, which can only be realized by mixing with odd crystal field terms (leads to ZPL emission, ZPL abbreviates zero-phonon line) or vibronic terms (results in stokes and anti-stokes sub-bands).[15] Generally, in Mn^{4+} heterovalent doping systems, the distorted $[MnF_6]$ octahedrons caused by the charge compensation defects can relax the selection rules, leading to a strong ZPL emission.[28] On the contrary, the PL profiles of heterovalent $(TMA)_2BO_2F_4$:Mn^{4+} are almost identical to that of commercial KSF equivalent systems.[30] The reason may be interpreted from two aspects: first, the $[MnF_6]^{2-}/[BO_2F_4]^{2-}$ chemical group substitution excludes the mixing of Mn-O vibronic modes, thereby the sub-bands coincide with KSF; second, the ZPL signal vanished

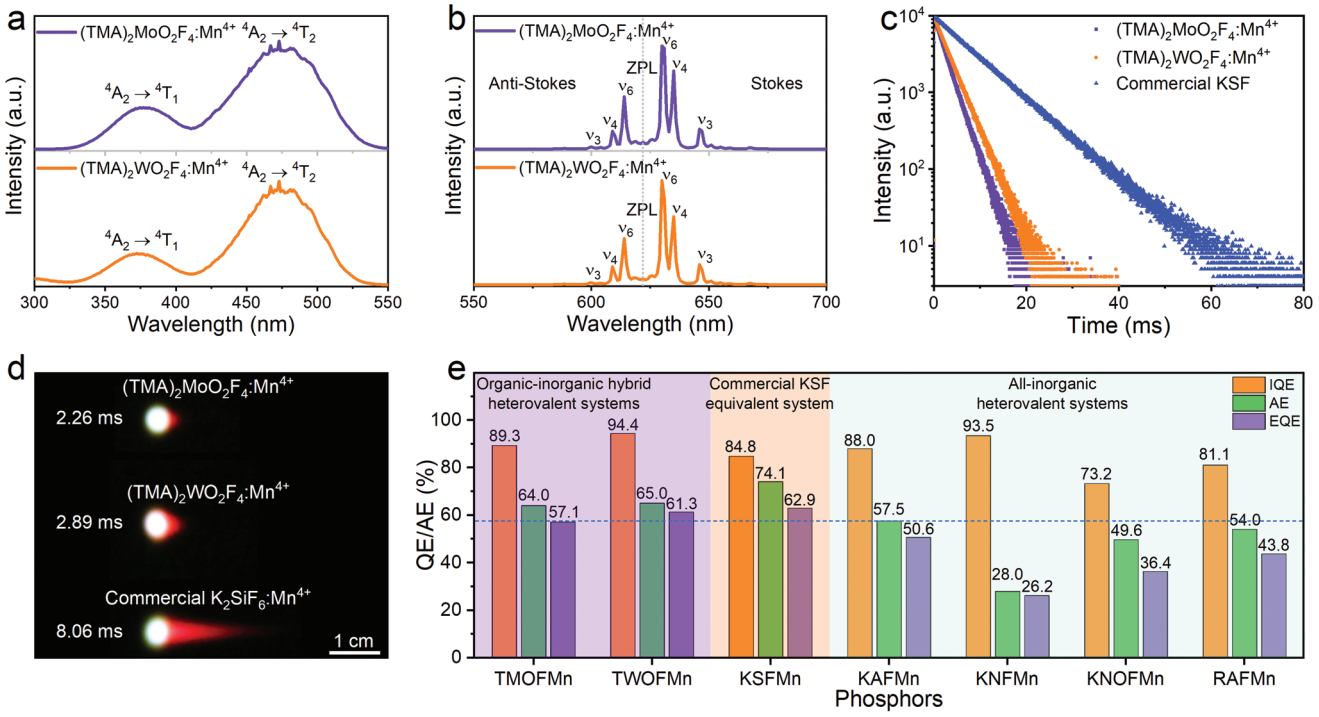

Figure 2. The a) PLE and b) PL spectra of $(TMA)_2BO_2F_4$:Mn^{4+}, and c) the PL decay curves of $(TMA)_2BO_2F_4$:Mn^{4+} and KSF as a reference. d) The luminescence tailing images of $(TMA)_2BO_2F_4$:Mn^{4+} and KSF. The phosphors mixed with resin were coated on paper, and a 375 nm laser spot scanned it at a horizontal speed of 1 m s^{-1}. e) The IQE, absorption efficiency (AE), and EQE of $(TMA)_2MoO_2F_4$:Mn^{4+} (TMOFMn), $(TMA)_2WO_2F_4$:Mn^{4+} (TWOFMn), and the commercial K_2SiF_6:Mn^{4+} (KSFMn) as well as the reported all-inorganic heterovalent Mn^{4+}-doped phosphors K_3AlF_6:Mn^{4+} (KAFMn), K_2NbF_7:Mn^{4+} (KNFMn), $K_3HF_2NbOF_5$:Mn^{4+} (KNOFMn), and Rb_3AlF_6:Mn^{4+} (RAFMn).

owing to the little structural distortion of $[MnF_6]$ secured by the absence of charge compensation defects. These spectral features prove the concept obtained from the aforementioned DFT simulations. In addition, a dramatical acceleration in PL decay was observed from $(TMA)_2BO_2F_4:Mn^{4+}$ with reference to KSF (Figure 2c), which is contributed by the low Mn^{4+}-site symmetry of $\bar{3}$ (C_{3i}).[24] The short lifetimes can greatly suppress the luminescence tailing phenomenon as illustrated in Figure 2d, which is beneficial for fast-response backlight display applications.[14] In addition, utilizing the difference in the PL lifetimes of $(TMA)_2BO_2F_4:Mn^{4+}$ and KSF, a novel time-resolved single-color multiplexing mode with high safety and easy access was designed for information security, which will be demonstrated later.

Empowered by the $[MnF_6]^{2-}/[BO_2F_4]^{2-}$ chemical group substitution and their 0D structure with remotely isolated octahedral groups, $(TMA)_2BO_2F_4:Mn^{4+}$ can also endure much higher Mn^{4+} doping concentration than traditional heterovalent systems (Table S1, Supporting Information). A series of pure $(TMA)_2BO_2F_4:Mn^{4+}$ phosphor samples doped with various Mn^{4+} doping concentrations (determined by inductively coupled plasma optical emission spectrometer) were synthesized successfully (Figure S13 and Table S12, Supporting Information). Taking $(TMA)_2WO_2F_4:Mn^{4+}$ as an example, the structural variations upon different Mn^{4+} doping concentrations were revealed by Rietveld refinements (Figures S14 and S15, and Table S13, Supporting Information). Figures S16 and S17, Supporting Information summarize the integrated intensity from their concentration-dependent PL spectra. The maximum PL intensity was found at ≈10 mol% Mn^{4+} contents, which is much higher than previously reported heterovalent doping systems (Table S1, Supporting Information). In the meantime, their decay lifetimes remain steady until reaching the optimal doping concentration. Upon heavier Mn^{4+} doping, the values only decrease slightly and remain in single-exponential decay throughout the series. Such results also evidence the suppression of the generation of charge compensation defects, implying the successful chemical group substitution. In addition, the internal QEs (IQEs) of $(TMA)_2MoO_2F_4:Mn^{4+}$ and $(TMA)_2WO_2F_4:Mn^{4+}$ can reach 89.3% and 94.4%, respectively, which is even higher than the commercial KSF (84.8%) phosphor as compared in Figure 2e. Some other representative Mn^{4+}-doped heterovalent phosphors may possess similarly high IQEs (right panels in Figure 2e), yet none of their external QEs (EQEs) can surpass 50%. Unprecedentedly, the EQEs of $(TMA)_2BO_2F_4:Mn^{4+}$ are close to that of KSF (57.1% and 61.3%, with reference to 62.9%).

The ultrahigh QEs of Mn^{4+} in heterovalent hosts can be assigned to the successful suppression of defect generations and inter-activator energy transfers, attributed to the "chemical group substitution" of $[MnF_6]^{2-}/[BO_2F_4]^{2-}$ groups and the "blocking effect" of organic spacers TMA^+, respectively. The mechanisms are schematically illustrated in **Figure 3**. For conventional all-inorganic systems (Figure 3a), the unwanted non-radiative energy transfer (cyan dotted arrow) and energy migration (purple dotted arrow) among activators and quenching sites co-exist with the radiative transition (red arrow), leading to considerable energy losses. Together with the populated quenching sites (charge compensation defects) in heterovalent doping hosts, Mn^{4+} luminescence will suffer from inferior QEs. For hybrid systems $(TMA)_2BO_2F_4:Mn^{4+}$ (Figure 3b), the large TMA^+ cations can effectively separate the inorganic blocks. Since both the energy transfer and energy migration processes rely on close spatial distance, they would be significantly suppressed, which is defined as the blocking effect (Figure 3b). Most importantly, the intrinsically prevented defect generation by the chemical group substitution strategy can further limit the energy loss. The synergistic coupling between the above two effects contributes to high luminescence efficiency.

The temperature-dependent luminescence properties of $(TMA)_2BO_2F_4:Mn^{4+}$ were investigated in detail (Figures S18–S21, Supporting Information). Similar to most of the Mn^{4+}-activated fluorides or oxyfluorides, both two compounds show anti-thermal quenching in the low-temperature zone (77–300 K) and normal thermal quenching in the high-temperature zone (25–200 °C).[5,31–33] On the other hand, compared to commercial KSF, $(TMA)_2BO_2F_4:Mn^{4+}$ experiences a severe luminescence quenching above 75 °C (Figure S22, Supporting Information). The inferior luminescent thermal stability is due to their relatively "soft" 0D crystal structure, which lacks structural rigidity compared with the KSF. Thanks to the high thermo-chemical

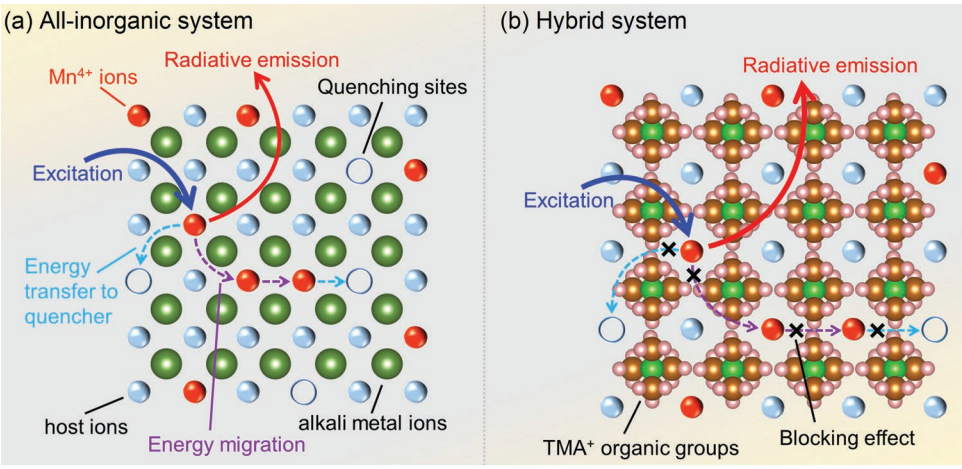

Figure 3. Schematic diagrams depicting the photoexcitation (blue arrow), energy migration (purple dotted arrow), energy transfer to quenching sites (cyan dotted arrow), and photoluminescence (red arrow) of Mn^{4+}-activated a) all-inorganic and b) organic-inorganic hybrid systems.

Figure 4. a) Illustrative diagram of the encrypted pattern design constructed by commercial KSF and as-prepared $(TMA)_2WO_2F_4:Mn^{4+}$, the designed general appearance and encrypted pattern, as well as the photo taken under natural light. b) Photos of the pattern captured at ≈0, ≈25, ≈50, ≈75, and ≈100 ms after the ≈365 nm light source is removed.

stability (without degradation up to 340 °C), their thermal quenching behaviors are reversible and reproducible as verified by several heating and cooling cycles (Figure S23, Supporting Information). Taking advantage of their different thermal quenching behavior from KSF, a single-color multiplexing mode based on temperature decoding was later developed for information security.

The high QEs, short PL lifetime, and narrow emission band make $(TMA)_2BO_2F_4:Mn^{4+}$ a promising emitter for backlight displays. As shown in Figure S24, Supporting Information, a prototype white light-emitting diode emits high-brightness white light with a luminous efficacy of 134.07 lm/W and a color gamut of 114.6% National Television System Committee (NTSC), showing an intriguing practical application prospect. Apart from lighting and display applications, phosphors have also been regarded as emerging materials for information security.[6,34–36] Benefiting from the comparable QEs (Figure S17, Supporting Information) and identical spectra (Figure S25, Supporting Information) to commercial KSF, the $(TMA)_2BO_2F_4:Mn^{4+}$ can be regarded as the lifetime-shortened and thermally quenched replicas of KSF. Therefore, it is difficult to distinguish them even with the help of luminescence spectral characterization. Consequently, the encrypted information based on them as anti-counterfeiting materials can be perfectly concealed. A highly secure and easy-access single-color multiplexing encryption pattern was then designed and fabricated with $(TMA)_2WO_2F_4:Mn^{4+}$ and KSF as a conceptual demonstration. As shown in **Figure 4**a, the encrypted code "2022" was hidden behind a general appearance of "8888", which is non-distinguishable under daylight (the right photo) or spectra analyses (Figure S25, Supporting Information). The information can only be decrypted in two ways (Figure 4b and Figure S26, Supporting Information, respectively, as well as Videos S1 and S2, Supporting Information), in neither case complex equipment such as a time gate is required. The former makes use of the lifetime difference of several milliseconds (Figure 2c); by using a commercial camera to capture photos continuously, the encrypted pattern can be revealed in the first several frames at 25, 50, and 75 ms after turning off the excitation lamp. The latter one involves the difference in the thermal quenching performance of KSF and $(TMA)_2WO_2F_4:Mn^{4+}$ (Figure S22, Supporting Information); as shown in the upper photo taken under ≈365 nm light irradiation, upon elevating temperatures as monitored by a thermal imager (lower photos), the encrypted information gradually emerges and becomes distinguishable at above 110 °C. After the temperature falls back to room temperature, the information can be sealed again, and the misleading pattern of "8888" reappears (last photo in Figure S26, Supporting Information).

3. Conclusion

In conclusion, we have proposed a novel "chemical group substitution" strategy to prevent the generation of charge compensation defects in heterovalent metal-ion doping systems. The strategy was demonstrated in $(TMA)_2BO_2F_4:Mn^{4+}$ from both theoretical and experimental aspects. The successful elimination of charge compensation defects in $(TMA)_2BO_2F_4:Mn^{4+}$ has greatly contributed to extremely high QEs (IQE up to 94.4%, EQE up to 61.3%) that are comparable to those of commercial red phosphor KSF (IQE = 84.8%, EQE = 62.9%). Utilizing the identical spectral features of $(TMA)_2BO_2F_4:Mn^{4+}$ and KSF as well as their differences in thermal quenching and PL decay lifetimes, a highly secure and easy-access single-color multiplexing encryption pattern was designed and demonstrated. The research provides an intriguingly new metal-ion doping scheme with the powerful potential of defect suppression and luminescence tuning, which can benefit the future developments of luminescent materials.

Supporting Information

Supporting Information is available from the Wiley Online Library or from the author.

Acknowledgements

This work was financially supported by the National Key Research and Development Program of China (2022YFB3503800), the National Science Foundation of China (Grant Nos. 52202170 and 51972117). This work was also funded by RFBR according to the research project No. 19-52-80003.

Conflict of Interest

The authors declare no conflict of interest.

Data Availability Statement

The data that support the findings of this study are available from the corresponding author upon reasonable request.

Keywords

defects, heterovalent substitution, Mn^{4+}, oxyfluoride, phosphors

Received: January 12, 2023
Revised: February 2, 2023
Published online: March 8, 2023

[1] M. Zhao, Q. Zhang, Z. Xia, *Acc Mater Res* **2020**, *1*, 137.
[2] A. Abdollahi, H. Roghani-Mamaqani, B. Razavi, M. Salami-Kalajahi, *ACS Nano* **2020**, *14*, 14417.
[3] B. Li, Y. Xu, X. Zhang, K. Han, J. Jin, Z. Xia, *Adv. Opt. Mater.* **2022**, *10*, 2102793.
[4] Y. Ou, W. Zhou, Z. Zhu, F. Ma, R. Zhou, F. Su, L. Zheng, L. Ma, H. Liang, *Angew. Chem., Int. Ed.* **2020**, *59*, 23810.
[5] T. Senden, R. J. A. van Dijk-Moes, A. Meijerink, *Light: Sci. Appl.* **2018**, *7*, 8.
[6] Y. Wang, Y. Zhou, H. Ming, Y. Zhao, E. Song, Q. Zhang, *ACS Appl. Mater. Interfaces* **2021**, *13*, 51255.
[7] Z. Xia, C. Ma, M. S. Molokeev, Q. Liu, K. Rickert, K. R. Poeppelmeier, *J. Am. Chem. Soc.* **2015**, *137*, 12494.
[8] J. Qiao, G. Zhou, Y. Zhou, Q. Zhang, Z. Xia, *Nat. Commun.* **2019**, *10*, 5267.
[9] H. X. Liao, M. Zhao, Y. Y. Zhou, M. S. Molokeev, Q. L. Liu, Q. Y. Zhang, Z. G. Xia, *Adv. Funct. Mater.* **2019**, *29*, 1901988.
[10] M. Zhao, H. Liao, L. Ning, Q. Zhang, Q. Liu, Z. Xia, *Adv. Mater.* **2018**, *30*, 1802489.
[11] S. X. Li, M. Amachraa, C. Chen, L. Wang, Z. B. Wang, S. P. Ong, R. J. Xie, *Matter* **2022**, *5*, 1924.
[12] M. Zhao, Z. Yang, L. Ning, Z. Xia, *Adv. Mater.* **2021**, *33*, 2101428.
[13] Y. H. Kim, P. Arunkumar, B. Y. Kim, S. Unithrattil, E. Kim, S. H. Moon, J. Y. Hyun, K. H. Kim, D. Lee, J. S. Lee, W. B. Im, *Nat. Mater.* **2017**, *16*, 543.
[14] Y. Y. Zhou, E. H. Song, M. G. Brik, Y. J. Wang, T. Hu, Z. G. Xia, Q. Y. Zhang, *J. Mater. Chem. C* **2019**, *7*, 9203.
[15] H. Zhu, C. C. Lin, W. Luo, S. Shu, Z. Liu, Y. Liu, J. Kong, E. Ma, Y. Cao, R. S. Liu, X. Chen, *Nat. Commun.* **2014**, *5*, 4312.
[16] J. Zhou, Y. Wang, Y. Chen, Y. Zhou, B. Milicevic, L. Zhou, J. Yan, J. Shi, R. S. Liu, M. Wu, *Angew. Chem., Int. Ed.* **2021**, *60*, 3940.
[17] X. D. Yi, R. F. Li, H. M. Zhu, J. Gao, W. W. You, Z. L. Gong, W. Guo, X. Y. Chen, *J. Mater. Chem. C* **2018**, *6*, 2069.
[18] E. Song, J. Wang, J. Shi, T. Deng, S. Ye, M. Peng, J. Wang, L. Wondraczek, Q. Zhang, *ACS Appl. Mater. Interfaces* **2017**, *9*, 8805.
[19] H. Lin, T. Hu, Q. Huang, Y. Cheng, B. Wang, J. Xu, J. Wang, Y. Wang, *Laser Photonics Rev.* **2017**, *11*, 1700148.
[20] D. Huang, H. Zhu, Z. Deng, Q. Zou, H. Lu, X. Yi, W. Guo, C. Lu, X. Chen, *Angew. Chem., Int. Ed.* **2019**, *58*, 3843.
[21] L. Huang, Y. Liu, S. Si, M. G. Brik, C. Wang, J. Wang, *Chem. Commun.* **2018**, *54*, 11857.
[22] L. Huang, Y. Liu, J. Yu, Y. Zhu, F. Pan, T. Xuan, M. G. Brik, C. Wang, J. Wang, *ACS Appl. Mater. Interfaces* **2018**, *10*, 18082.
[23] L. Huang, Y. Zhu, X. Zhang, R. Zou, F. Pan, J. Wang, M. Wu, *Chem. Mater.* **2016**, *28*, 1495.
[24] H. Ming, Y. F. Zhao, Y. Y. Zhou, M. S. Molokeev, Y. J. Wang, S. Zhang, E. H. Song, S. Ye, Z. G. Xia, Q. Y. Zhang, *Adv. Opt. Mater.* **2022**, *10*, 2102141.
[25] S. Zhang, Y. F. Zhao, J. D. Zhou, H. Ming, C. H. Wang, X. P. Jing, S. Ye, Q. Y. Zhang, *Chem. Eng. J.* **2021**, *421*, 129886.
[26] T. Hu, H. Lin, Y. Cheng, Q. Huang, J. Xu, Y. Gao, J. Wang, Y. Wang, *J. Mater. Chem. C* **2017**, *5*, 10524.
[27] Y. Zhou, S. Zhang, X. Wang, H. Jiao, *Inorg. Chem.* **2019**, *58*, 4412.
[28] Y. Y. Zhou, H. Ming, S. Zhang, T. T. Deng, E. H. Song, Q. Y. Zhang, *Chem. Eng. J.* **2021**, *415*, 128974.
[29] P. Arunkumar, H. B. Cho, K. H. Gil, S. Unithrattil, Y. H. Kim, W. B. Im, *Nat. Commun.* **2018**, *9*, 4691.
[30] P. P. Wan, Z. J. Liang, P. L. Luo, S. X. Lian, W. L. Zhou, R. S. Liu, *Chem. Eng. J.* **2021**, *426*, 131350.
[31] L. Huang, S. Lou, L. Cao, B. Liu, Y. Zhu, Y. Liu, C. Wang, J. Wang, *ACS Mater. Lett.* **2022**, *4*, 1716.
[32] S. G. He, F. F. Xu, T. T. Han, Z. Q. Lu, W. Wang, J. Q. Peng, F. Du, F. L. Yang, X. Y. Ye, *Chem. Eng. J.* **2020**, *392*, 123657.
[33] J. B. Zhou, Y. Y. Chen, C. Y. Jiang, B. Milicevic, M. S. Molokeev, M. G. Brik, I. A. Bobrikov, J. Yan, J. H. Li, M. M. Wu, *Chem. Eng. J.* **2021**, *405*, 126678.
[34] B. Li, J. Jin, M. Yin, X. Zhang, M. S. Molokeev, Z. Xia, Y. Xu, *Angew. Chem., Int. Ed.* **2022**, *61*, 202212741; *Angew. Chem.* **2022**, *134*, 202212741.
[35] X. Huang, Q. Guo, D. Yang, X. Xiao, X. Liu, Z. Xia, F. Fan, J. Qiu, G. Dong, *Nat. Photonics* **2019**, *14*, 82.
[36] X. Liu, Y. Wang, X. Li, Z. Yi, R. Deng, L. Liang, X. Xie, D. T. B. Loong, S. Song, D. Fan, A. H. All, H. Zhang, L. Huang, X. Liu, *Nat. Commun.* **2017**, *8*, 899.

